SIM-Lite Mission Spectral Calibration Sensitivities and Refinements

C. Zhai, X. An, R. Goullioud, B. Nemati, M. Shao, J. Shen, U. Wehmeier, X. Wang, M. Weiler, T. Werne, and J. Wu

Jet Propulsion Laboratory, California Institute of Technology, Pasadena, CA 91109

ABSTRACT

SIM-Lite missions will perform astrometry at microarcsecond accuracy using star light interferometry. For typical baselines that are shorter than 10 meters, this requires to measure optical path difference (OPD) accurate to tens of picometers calling for highly accurate calibration. A major challenge is to calibrate the star spectral dependency in fringe measurements — the spectral calibration. Previously, we have developed a spectral calibration and estimation scheme achieving picometer level accuracy. In this paper, we present the improvements regarding the application of this scheme from sensitivity studies. Data from the SIM Spectral Calibration Development Unit (SCDU) test facility shows that the fringe OPD is very sensitive to pointings of both beams from the two arms of the interferometer. This sensitivity coupled with a systematic pointing error provides a mechanism to explain the bias changes in 2007. Improving system alignment can effectively reduce this sensitivity and thus errors due to pointing errors. Modeling this sensitivity can lead to further improvement in data processing. We then investigate the sensitivity to a model parameter, the bandwidth used in the fringe model, which presents an interesting trade between systematic and random errors. Finally we show the mitigation of calibration errors due to system drifts by interpolating instrument calibrations. These improvements enable us to use SCDU data to demonstrate that SIM-Lite missions can meet the 1pm noise floor requirement for detecting earth-like exoplanets.

Keywords: Interferometry, instrument calibration, fringe phase estimation, wave front aberration

1. INTRODUCTION

In 2007, the SIM PlanetQuest Spectral Calibration Development Unit (SCDU)[1] successfully demonstrated that spectral calibration can be done better than 20pm in estimating change of optical path difference (OPD) between two different source spectra (*spectral delay change*). A calibration scheme and OPD estimation algorithm was developed then for achieving the SIM PlanetQuest Engineering Milestone 4(EM4). Since then, the SCDU test facility has been used to study system sensitivities to various physical parameters and understand the mechanism for the bias changes[1] to further improve the the performance. It is convenient to divide the calibration errors into three portions, namely model errors, errors due to system instability, and random errors. In the paper, we present results from studying, understanding and improving the system regarding mainly on the model errors and errors due to instability.

The pointing of both beams from the two arms of the interferometer is one of the most sensitive physical parameters for SCDU. The pointing of the beams directly affects the locations of the images at fringe tracking camera (FTC). To the first order, we use a linear model to address fringe OPD sensitivity to the pointings and call the linear responses in OPD errors to the pointing errors *pointing sensitivities*. Systematic pointing errors lead to systematic OPD errors. One of the important systematic pointing errors comes from estimating the spot centroid using finite sampling of image over a limited region on the CCD of angle tracking camera (ATC). Because the error depends on color, we call this *color dependent centroid shifts* (CDCS). See reference[3] for details. The pointing error due to CDCS was about 0.2μrad. The pointing sensitivities can easily change by 0.1nm/μrad leading to 20pm picometer level OPD bias changes. This explains the shifts of the biases observed in 2007[1] and why the biases varied significantly across different spectral channels because the pointing sensitivities strongly depend on the spectral channels. Instrument alignment procedures are developed to systematically reduce the

Send correspondence to C.Z.: E-mail: chengxing.zhai@jpl.nasa.gov

pointing sensitivities. Improving the pointing sensitivities not only reduces systematic errors, e.g. the residual CDCS errors, but also mitigates the errors from system pointing drifts and random pointing fluctuations.

Our next improvement is tuning a model parameter used in spectral calibration. The fringe model plays a central role in the spectral calibration. A crucial parameter in the fringe model is the bandwidth over which we perform the integration to synthesize fringes. In absence of random errors, we like to use a bandwidth as broad as possible to minimize truncation errors. Practically, due to random uncertainties, as we increase the bandwidth to include weak signals, the noises we pick up may be larger than the signal itself. Therefore, this requires us to balance systematic and random errors. We determine the bandwidth by minimizing the RMS of the total error.

As the system drifts, the instrument state changes between epochs when we calibrate the system and when we do the observations. This instrument state change leads to calibration error. For SIM, nominally, we perform daily instrument calibrations. Because most of the drifts are thermally driven and happen over a typical time scale of a day, we employ a linear interpolation on the instrument calibrations to remove calibration errors due to linear drifts.

With all these improvements, the Allan deviations of the SCDU biases show that the biases do average down below 1pm meeting the noise floor requirement for SIM-Lite missions to detect earth-like planets.[4,5]

2. REVIEW OF THE BASIC MODEL AND END-TO-END CALIBRATION PROCEDURE

The spectral dependency in fringes is the driving force for spectral calibration. For picometer accuracy, even for the narrowest spectral channel that consists only one pixel along the spectral direction, the effective fringe phase can still depend on the source spectra at hundreds of picometer level.[2] It is crucial to capture the spectral dependency in the fringe model. We call the fringe model that includes the source spectral effect, *broadband fringe model* or *white light fringe model*.

2.1 Broadband fringe model and long stroke calibration

Broadband fringe may be modeled as an incoherent superposition of the monochromatic fringes with the intensity proportional to the source spectral energy function and the system throughput. Let $y_i^{\rm p}$ be CCD count rate detected by a spectral channel p per sample period for i-th sampling interval and u_i be the average OPD as measured by internal metrology. The fringe model may be expressed as

$$y_i^{\rm p} = I_{\rm DC}^{\rm p} + \int_0^\infty dk S_{\rm source}(k) T^{\rm p}(k) V^{\rm p}(k) \cos[k u_i + \phi^{\rm p}(k)] \tag{1}$$

where $S_{\rm source}(k)$ is the source spectral energy density function with k being the wave number of the photon; $T^{\rm p}(k)$ is the system throughput for the spectral channel p including CCD quantum efficiency (QE); $V^{\rm p}(k)$ and $\phi^{\rm p}(k)$ are the fringe visibility and phase for the spectral channel p respectively. Physically, there are several contributors to the phase dispersion $\phi^{\rm p}(k)$. The imbalanced bulk material and coatings between the two arms yields smooth phase dispersion depending only on the wave number. The wave front errors, however, make the fringe phases $\phi^{\rm p}(k)$ depending not only the photon wave number k, but also the spectral channel p used for detection. Eq. (1) assumes staircase modulation. For a triangular modulation profile as used by SCDU, an extra multiplicative "sinc" factor is needed for the visibility function, *i. e.* $V^{\rm p}(k) \to V^{\rm p}(k){\rm sinc}(k\Delta u/2)$ where Δu is the dithering step size. For the reason of simplicity, we shall hide this "sinc" factor.

To model the fringe using Eq. (1), the required input parameters are the DC intensity $I_{\rm DC}^{\rm p}$, the amplitude

$$A_{\rm source}^{\rm p}(k) \equiv S_{\rm source}(k) T^{\rm p}(k) V^{\rm p}(k)\,, \tag{2}$$

and the phases $\phi^{\rm p}(k)$, which are measured by calibration. We now show that all these three input parameters can be calibrated using fringe measurements over a large OPD range, which we shall call *long stroke fringe* measurements. The DC fringe intensities can be easily estimated by taking an average of a long stroke fringe signals, for example. The calibration of amplitude $A_{\rm source}^{\rm p}$ and $\phi^{\rm p}(k)$ is a little involved. Treating $y_i^{\rm p}$ as a

function u_i, model (1) resembles the structure of a Fourier integral. The Fourier transform of the fringe signal $y_i^{\rm p}$ as function of u_i yields a complex response function $\tilde{y}(k)$, whose amplitude is proportional to the product of the spectral energy distribution, the throughput, and the visibility and whose phase is the phase dispersion function, *i.e.*

$$\tilde{y}(k) = \pi S_{\rm source}(k) T^{\rm p}(k) V^{\rm p}(k) e^{i\phi^{\rm p}(k)} \,. \tag{3}$$

In view of Eq. (3), the amplitude $A^{\rm p}_{\rm source}(k)$ and phase $\phi^{\rm p}(k)$ may be estimated by the Fourier transform of the fringe signal. We use Discrete Fourier Transform (DFT) of the long stroke fringe as an estimate of the Fourier transform of the fringe signal. The spectral resolution in wave number is determined by the stroke length L (OPD range) of the long stroke fringe measurements, via $\Delta k = 2\pi/L$. Because of wavefront aberrations, $\phi^{\rm p}(k)$ varies by tens of nanometers across the bandwidth of a SCDU spectral pixel. We require the stroke length to be large enough to resolve the phase variation of function $\phi^{\rm p}(k)$. We get the following fundamental relations for SIM-Lite mission spectral calibration:

$$A^{\rm p}_{\rm source}(k) = \frac{1}{\pi}|\tilde{y}(k)| \approx \frac{1}{\pi}|\tilde{y}^{\rm p}_{\rm DFT}(k)| \,, \quad \phi^{\rm p}(k) = {\rm Arg}\{\tilde{y}(k)\} \approx {\rm Arg}\{\tilde{y}^{\rm p}_{\rm DFT}(k)\} \,. \tag{4}$$

Using DFTs, the continuous integration in model (1) becomes a summation over a set of discretized wave numbers $k_m = m\Delta k$ that are multiples of the wave number quanta Δk as

$$y_i^{\rm p} \approx I^{\rm p}_{\rm DC-cal} + \sum_{m=M_-}^{M_+} A^{\rm p}_m \cos[k_m u_i + \Phi^{\rm p}_m] \tag{5}$$

where $A^{\rm p}_m, \Phi^{\rm p}_m$ are related to the DFT of the fringe signal $\tilde{y}^{\rm p}_{\rm DFT}(k)$ by

$$A^{\rm p}_m = \Delta k A^{\rm p}_{\rm source}(k_m) = \Delta k |\tilde{y}^{\rm p}_{\rm DFT}(k_m)|/\pi \,, \quad \Phi^{\rm p}_m = {\rm Arg}\{\tilde{y}^{\rm p}_{\rm DFT}(k_m)\} \tag{6}$$

assuming bandwidth $[M_-\Delta k, M_+\Delta k]$ contains sufficient amount of signal. We shall discuss how to choose this bandwidth later in section 3.2.

2.2 Instrument and spectral ratio calibration

A long stroke DFT calibration can effectively measure the complex spectral response. Measuring the complex spectral response for each observation target, however, is not feasible simply because it takes too much mission time especially for relatively dimmer targets. To have a flight viable calibration scheme, we separate the total spectral calibration into *instrument calibration* and *source spectral calibration*. The instrument calibration measures the complex spectral channel response using a bright source while the spectral calibration measures the spectral ratio between the observation target and the calibration source. To illustrate this, we write the discrete form of the fringe model as

$$\begin{aligned} y_{\rm obs}(u) \;&=\; I^{\rm obs}_{\rm DC} + \sum_{m=M_-}^{M_+} A^{\rm p,obs}_m \cos\left[k_m u + \Phi^{\rm p,obs}_m\right] = I^{\rm obs}_{\rm DC} + \sum_{m=M_-}^{M_+} \left(A^{\rm p,obs}_m / A^{\rm p,cal}_m\right) A^{\rm p,cal}_m \cos\left[k_m u + \Phi^{\rm p,obs}_m\right] \\ &\approx\; I^{\rm obs}_{\rm DC} + \sum_{m=M_-}^{M_+} \left(A^{\rm p,obs}_m / A^{\rm p,cal}_m\right) A^{\rm p,cal}_m \cos\left[k_m u + \Phi^{\rm p,cal}_m\right] \,, \end{aligned} \tag{7}$$

where the instrument calibration estimates $A^{\rm p,cal}_m$ and $\Phi^{\rm p,cal}_m$ and the spectral ratio is estimated by the ratio $A^{\rm p,obs}_m / A^{\rm p,cal}_m \approx S_{\rm obs}(k_m)/S_{\rm cal}(k_m)$. Because the spectral calibration is very sensitive to to the phase of the complex spectral response, we use a bright source to calibration the instrument to save time. On the other hand, the spectral ratio is relatively stable, therefore, it is sufficient to perform the star spectral calibration once per mission per star.

2.3 End-to-end calibration procedure

The spectral calibration is based on a model of the broadband fringe. Since the fringe is a function of OPD, this model can be used to produce an OPD estimate by finding the OPD at which the model fringe best matches the observed fringes. The solution can be found iteratively. Because fringe OPD estimation involves synthesizing fringes using calibration data and comparing model and observation fringes, the spectral calibration and fringe estimation are strongly coupled. We refer to the whole process of using observation and calibration data to estimate the fringe OPD as *end-to-end calibration*. The data set for end-to-end calibration includes both the narrow angle observation fringe data and the calibration data set. SCDU uses a tungsten lamp plus filters to simulate different source spectra. The narrow angle observations are performed by chopping between two filters (nominally KG03 and BG38) while applying 1.32 um (short stroke) OPD modulation. The calibration data set includes long stroke instrument calibration measurements plus the long stroke spectral ratio calibration measurements. For instrument calibration, we simply use the tungsten lamp without any filter, which we call *open* filter, to simulate a bright calibration star. Spectral ratios for KG03 and BG38 with respect to open filter are measured by taking long stroke fringe measurements for cases with KG03, BG38 and open filters. The ratios of the amplitudes of the DFTs of the fringe signals give the corresponding spectral ratios. For each SCDU experiment, the fringe data consists of the fringe signals y_i (CCD counts) and the corresponding internal metrology measurements u_i, where i is the sample index. Internal metrology measures the OPD profile for the phase modulation. There is a separate set of data for each of the two polarizations and each spectral channel.

The overall data flow is summarized in Fig. 1. We first perform DFT of the long stroke instrument fringe signal to estimate the amplitude $A_m^{\rm cal}$ and the phase $\Phi_m^{\rm cal}$ for each spectral bin. We then compute the spectral ratios $A_m^{\rm obs}/A_m^{\rm cal}$ for two nominal filters, BG38 and KG03, respectively using DFTs of the long stroke fringes from the spectral ratio calibration. With the instrument calibration and the spectral ratio calibration, we start with an initial OPD, which is only required to be correct within a half of the effective wavelength of the broadband fringe signal to avoid phase wrapping ambiguity. The fringe model is used to synthesize fringes corresponding to this initial OPD and the modulation profile u_i measured by the internal metrology. The narrow angle observation fringes are then compared with the synthesized fringes to form an estimate of the delay offset between the observation and model fringes. This offset is fed back to the fringe model to update the OPD used in the fringe computation at the previous step. The refined model fringe is then compared with the observation. The process stops when the delay offset between the model and observation fringes is smaller than a threshold d_ϵ, *e.g.* 1pm, and the OPD used in this last fringe computation is the OPD estimate for the observed fringe set.

3. SPECTRAL CALIBRATION ERRORS AND IMPROVEMENTS

It is convenient to break down the total spectral calibration error $\epsilon_{\rm tot}$ into errors intrinsic to narrow angle observations $\epsilon_{\rm NA}$, model errors $\epsilon_{\rm model}$, random errors $\epsilon_{\rm random}$, and errors due to system drift $\epsilon_{\rm drift}$ as

$$\epsilon_{\rm tot} = \epsilon_{\rm NA} + \epsilon_{\rm model} + \epsilon_{\rm drift} + \epsilon_{\rm random} \,. \tag{8}$$

$\epsilon_{\rm NA}$ includes errors in narrow angle observations not related to spectral changes. For example, the system drift between observing target star and reference stars. $\epsilon_{\rm model}$ includes systematic errors due to inaccuracy of model and limitation from practical implementation. Examples are using DFTs to represent Fourier Transform or ignoring ghost reflections, metrology cyclic errors. $\epsilon_{\rm drift}$ represents errors due to system changes. For example, the system states at the instrument calibrations and the system states at observations may be different. $\epsilon_{\rm random}$ includes errors due to photon shot noise or errors due to pseudo-random vibrations. In the following, we shall address mainly model errors $\epsilon_{\rm model}$ and errors due to system drifts $\epsilon_{\rm drift}$.

3.1 Sensitivity to pointing errors

For interferometry, alignment is very crucial for achieving high performance. The fringes are measured in focal plane of fringe tracking camera (FTC). Because the size of diffraction spot (similar to Airy spot) is smaller than the pixel, the fringe measurements are sensitive to the location on FTC to a small fraction of a pixel. The fringe model assumes fringe placement on FTC is fixed, therefore, changes in this placement lead to model errors ($\epsilon_{\rm model}$). The fringe images are formed by interfering light from two arms (left and right arms). Because

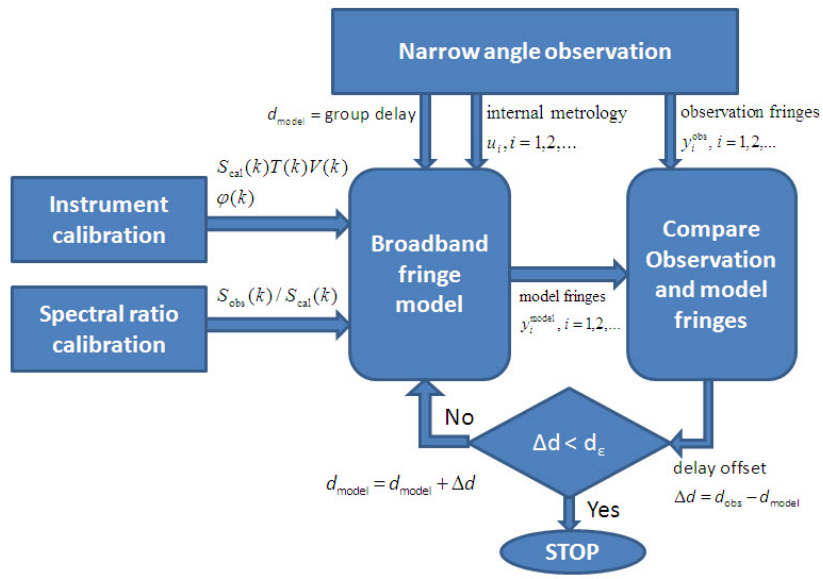

Figure 1. SCDU Spectral calibration flow chart

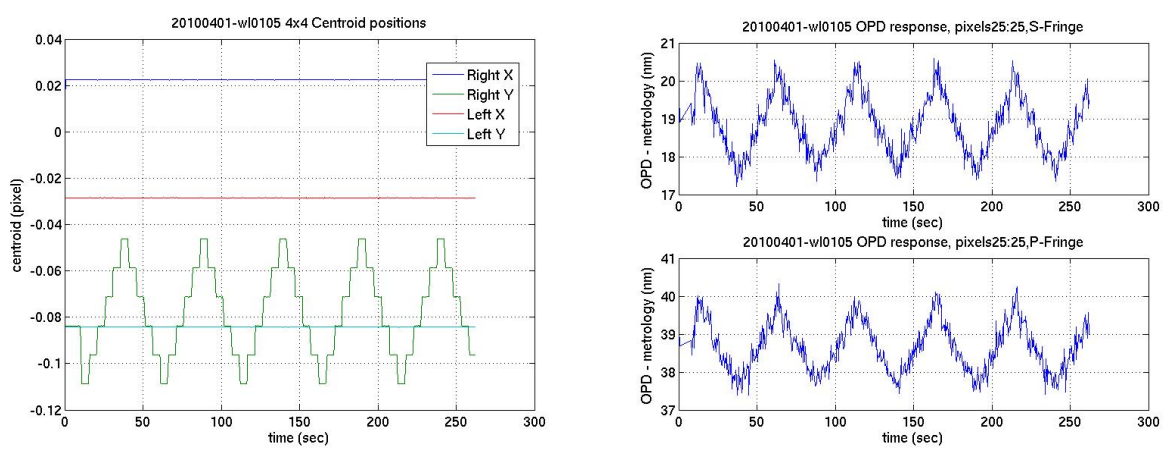

Figure 2. The pointing modulation profile as measured by the centroids of images on angle tracking camera.(left)). Channel OPD responses to the pointing modulation for open filter source spectrum (right, up for s-fringe, bottom for p-fringe).

the pointing of each arm can vary independently in two directions (x and y) on CCD, there are totally four independent pointing variations and thus four corresponding sensitivities.

We measure the four pointing sensitivities by modulating the pointing of left and right arms along x and y directions separately and observing the fringe phase responses. The experiments were done with short stroke fringe measurements as done for the nominal narrow angle observations. The left plot in Fig. 2 shows a typical triangular staircase modulation pattern with step size 1/80 pixel = 0.5μrad (1pixel = 40μrad) in the pointing for left arm along y direction. We use the narrowest spectral channels, which consist only one pixel along the spectral direction and five pixels along the direction perpendicular to the spectral direction. The fringe phase responses for both s- and p-polarization fringes from pixel channel 25 are shown in the two plots at right in Fig. 2. We use a linear response model to characterize the sensitivities:

$$d_i^{\mathrm{p}} = \alpha_i^{\mathrm{p}} \Delta\theta + d_0^{\mathrm{p}}\,, i = L_x, L_y, R_x, R_y\,, \tag{9}$$

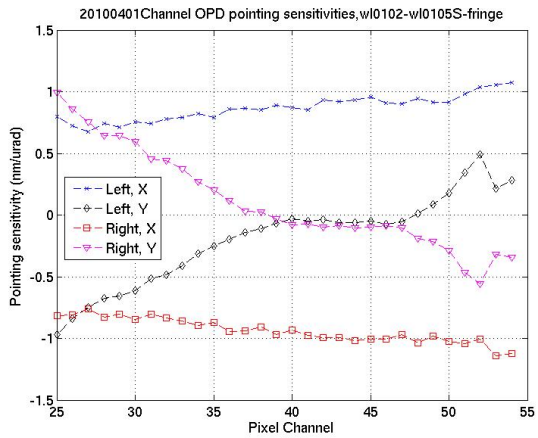

;

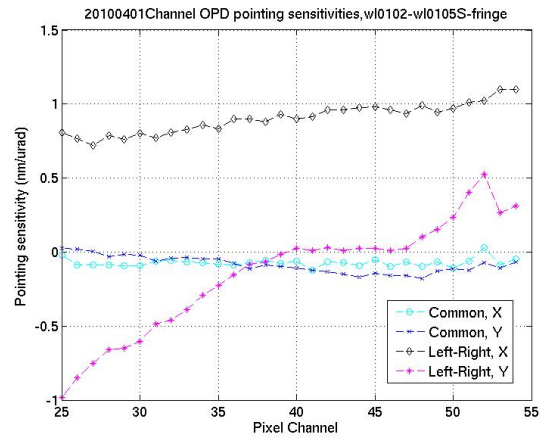

;

Figure 3. The linear responses of OPDs to four pointing variations, for left and right arms along x and y directions respectively(left). The linear responses of OPDs to common pointing variations and differential pointing variations (right).

where superscript p represents the pixel spectral channel, and subscript i labels one of the four pointing variations, left arm along x direction, L_x, left arm along y direction, L_y, right arm along x direction, R_x, and right arm along y direction, R_y. d_0^{p} is the delay for channel p without any pointing modulation. α_i^{p} is the pointing sensitivity of channel p OPD in response to i-th pointing variation. The sensitivities α_i^{p} for pixel spectral channels $p = 25, 26, \cdots, 54$. are displayed in Fig. 3. We group the sensitivities in two ways. The left plot shows sensitivities to pointings of each arm along x or y directions individually while the right plot shows the sensitivities to common pointing changes of both arms along x and y directions and differential pointing changes between two arms along x and y directions respectively *i.e.*

$$\alpha^{\mathrm{p}}_{\mathrm{common_x}} = \alpha^{\mathrm{p}}_{L_x} + \alpha^{\mathrm{p}}_{R_x}\,, \alpha^{\mathrm{p}}_{\mathrm{common_y}} = \alpha^{\mathrm{p}}_{L_y} + \alpha^{\mathrm{p}}_{R_y}\,,\ \alpha^{\mathrm{p}}_{\mathrm{diff_x}} = \frac{1}{2}\left(\alpha^{\mathrm{p}}_{L_x} - \alpha^{\mathrm{p}}_{R_x}\right)\,, \alpha^{\mathrm{p}}_{\mathrm{diff_y}} = \frac{1}{2}\left(\alpha^{\mathrm{p}}_{L_y} - \alpha^{\mathrm{p}}_{R_y}\right)\,. \tag{10}$$

It is easy to see that the sensitivities to the differential pointing changes are much larger than that to common pointing changes. This is expected because the fringe phases represent the optical path difference between the two arms, therefore it is more sensitive to differential pointing changes. We note that the pointing sensitivities depend on the spectral channels and thus is not a pure geometric effect.

In 2007, we observed unexplained changes in the biases.[1] The biases can shift by more than 20 picometers after realigning the systems. We also observed large variations of the biases across the spectral channels. Fig. 4 displays two plots showing the channel biases after spectral calibration for two experiments. Between the two experiments, the mean biases for both s- and p-polarization fringes shifted by more than 20pm. For the experiment with small mean biases (right plot), the variations of individual channel biases are large showing evidence of systematic errors.

We now explain these changes using systematic pointing errors coupled with pointing sensitivities. Our nominal experiments in 2007 all suffered systematic pointing errors due to *color dependent centriod shifts*(CDCS).[3] SCDU controls the pointing of two beams from the two arms based on the beam centriods measured by angle tracking camera (ATC). Because the centroid is sampled by pixels of finite size over a finite region, the traditional centroid estimation algorithm has systematic error depending on the wavelength or source spectra because the size of diffraction spot on the ATC is proportional to wavelength. This is especially true when there are significant wavefront aberrations causing the spot to be asymmetric. Because the systematic error depends on the wavelength, the systematic errors are different for different spectra. As we change the source spectra, the pointing of the beams changes. SCDU uses three PZT actuators to control each siderostat to steer each beam. Fig. 5 shows the PZT voltage changes during a typical narrow angle run in 2007 in response to switching filters due to CDCS. The voltage changes indicate that the pointing changes between two filters are approximately

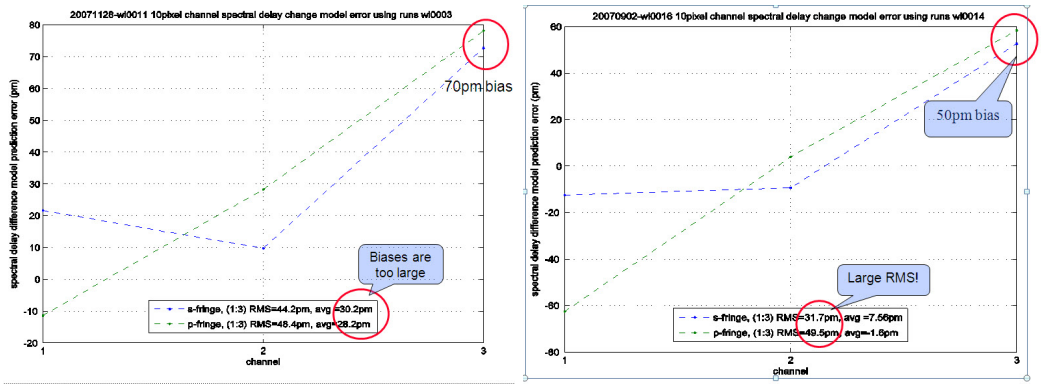

Figure 4. Mean channel biases after spectral calibration can be large (left). Even thought the mean biases are small, channel biases varies significantly across different spectral channels(right).

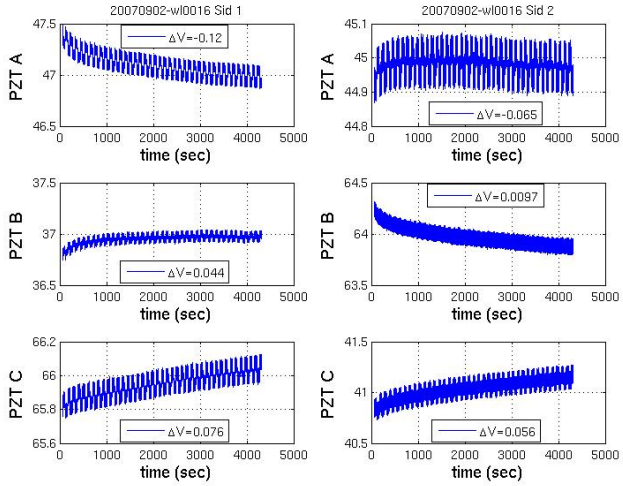

;

Figure 5. PZT voltages of the siderostats show the pointing changes between two filters for a typical narrow angle experiment in 2007.

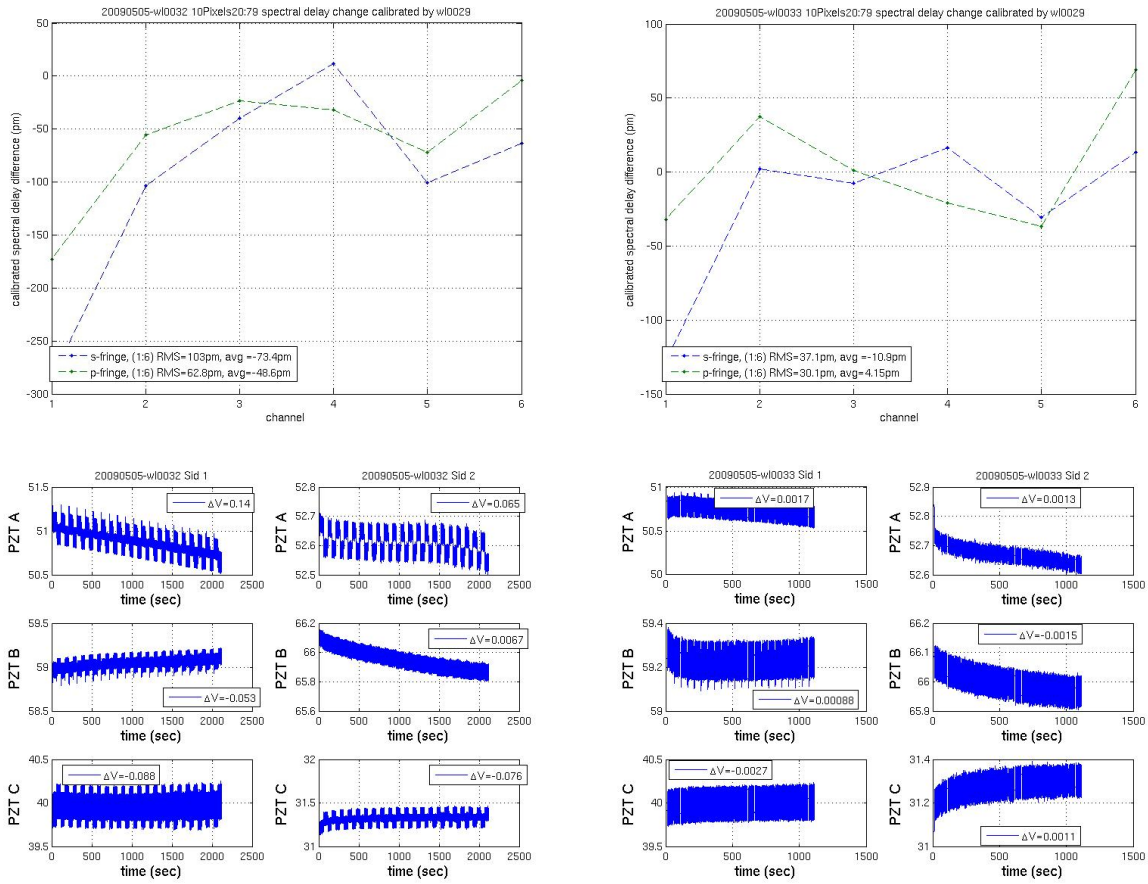

Figure 6. The channel OPD biases after calibration with (up, left) and without (up,right) CDCS. The corresponding PZT voltages are shown in plots at bottom with CDCS (left), without CDCS(right) .

0.2μrad (1volt $\sim$ 2μrad). The pointing sensitivities are typically between 0.1nm/μrad–1nm/μrad. For pointing error of 0.2μrad, pointing sensitivity of 0.1nm/μrad gives 0.1nm/μrad $\times$ 0.2μrad = 20pm error in OPD. Because the pointing sensitivities can easily vary by 0.1nm/μrad between alignments and the differences between different spectral channels are also in multiples of 0.1nm/μrad, the systematic errors due to CDCS explains naturally the bias shifts and the large variations of the channel biases across spectral channels observed in 2007. We measured the pointing error due to CDCS and was able to compensate the CDCS using an offset pointing technique in operation. Fig. 6 shows both the channel OPD biases (up) and the corresponding PZT voltages (bottom) for experiments with CDCS (left) and with CDCS compensated (right) respectively. When there is CDCS error, not only the biases can become large but also the the OPDs tend to vary more between spectral channels. With the CDCS compensated, the narrow angle biases does not show large systematic variations across spectral channels. Note that the systematic pointing error is less than 0.01urad after compensating CDCS.

Our alignment procedure effectively reduces pointing sensitivities. Fig. 7 displays a typical set of pointing sensitivities after aligning the system to minimize the pointing sensitivity. The overall pointing sensitivities are reduced significantly from the sensitivity shown in Fig. 3. Due to spectral dependency, we can only align the system so that the average of the sensitivities over spectral channels is minimized. Because the CDCS can be compensated to 0.01μrad accuracy and the pointing sensitivities are generally reduced to less than 0.3nm/μrad, the systematic error due to CDCS should be less than 3pm.

We move on further to model the pointing sensitivities using long stroke fringes measured at different pointings. This enables us to estimate pointing sensitives and OPD errors associated with pointing errors using the

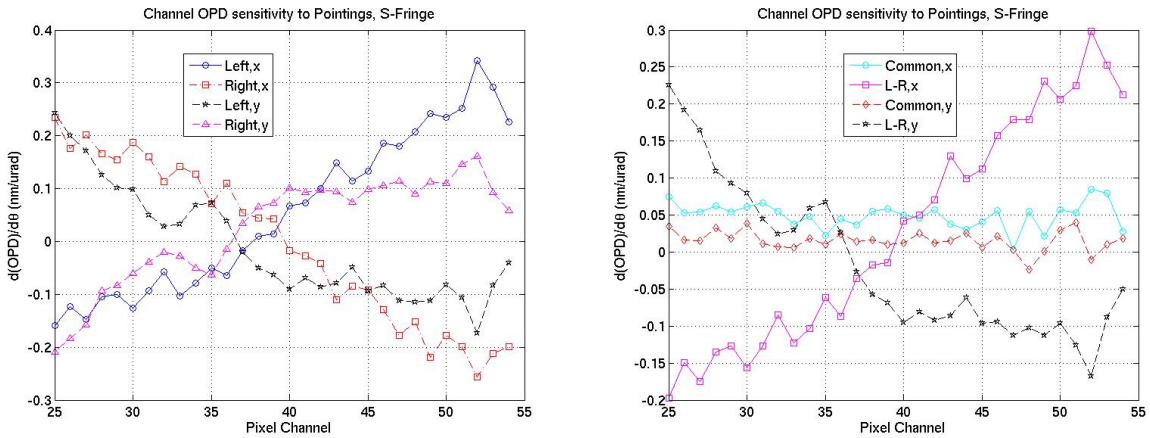

Figure 7. The linear response of OPD to pointing changes of each arm along x and y directions(left) and common and differential responses (right).

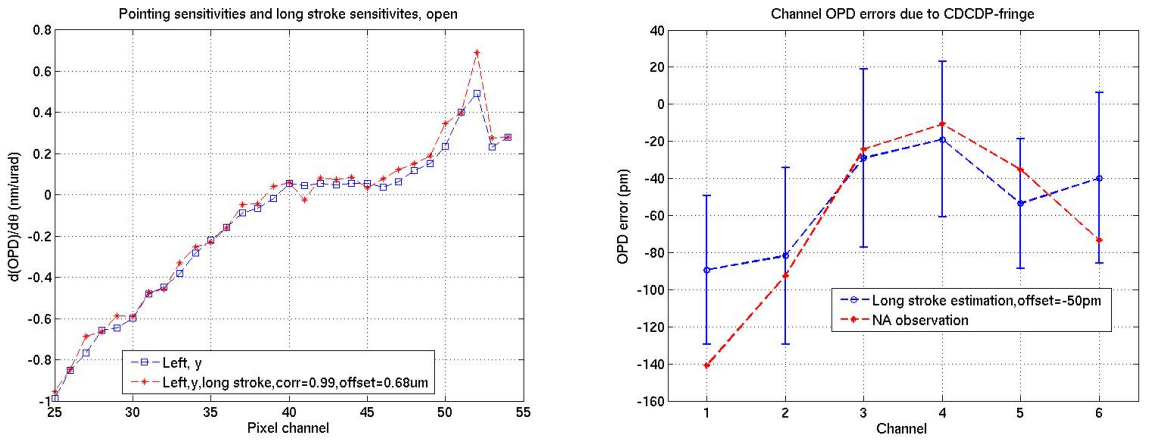

Figure 8. Pointing sensitivities in response to left arm pointing change along y direction, estimated and measured (left). Systematic OPD errors due to CDCS, estimated and measured (right).

fringe model. Fig. 8 displays the pointing sensitivities (left) and systematic channel OPD errors (right) due to CDCS estimated using long stroke fringe measurements at different pointings. The estimated pointing sensitivities using long stroke fringe measurements and fringe model agrees very well with the measured sensitivities (correlation = 0.99) up to a geometric offset about 680nm. These are due to system drifts between two different long stroke experiments which are separated by about 3 hours and 40 minutes. The channel OPD systematic errors also has an offset of -50pm. Future improvement may be achieved by conducting a series of these measurements close in time to remove most of the drifts. The left plot in Fig. 9 shows the estimated pointing sensitivities for open filter, KG03, and BG38, using long stroke fringe measurements at different pointings. We note that pointing sensitivities depend on the source spectra. The differences between filters in the pointing sensitivities give the sensitivity of OPD calibration error to pointing drift between instrument calibration and narrow angle observation. The right plot in Fig. 9 shows the systematic OPD errors due to pointing change for the left arm along y direction by 0.02pixel between instrument calibration and observation. The estimated errors (connected with dashed lines) agree well with the narrow angle measurements (individual squares and circles) for both polarization states. Pointing errors affect narrow angle observation accuracy in two ways. First of all, the differential error, *e.g*, the CDCS directly leads to errors in narrow chop biases. Secondly, because the pointing sensitivity depends on color. This leads to the calibration errors when the pointing for instrument calibrations

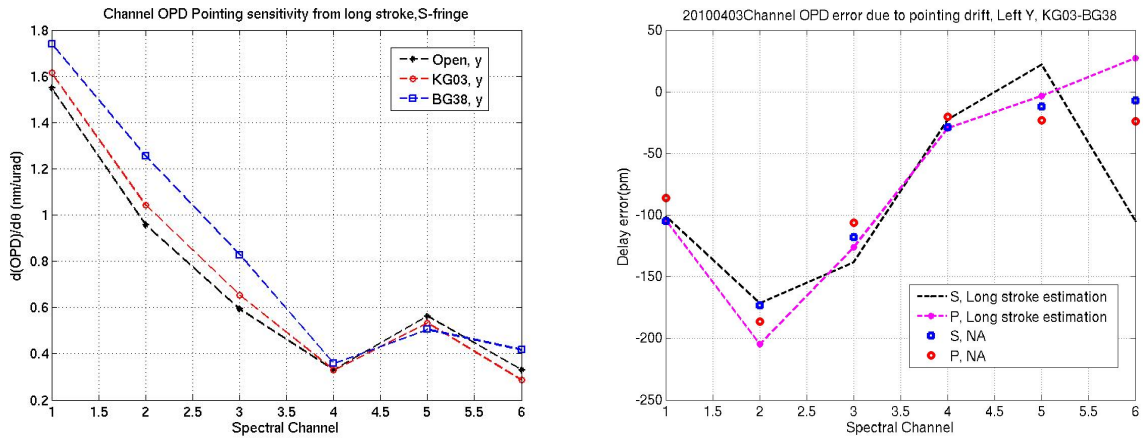

Figure 9. Pointing sensitivities in response to left arm pointing change along y direction, estimated and measured (left). Systematic OPD errors due to CDCS, estimated and measured (right).

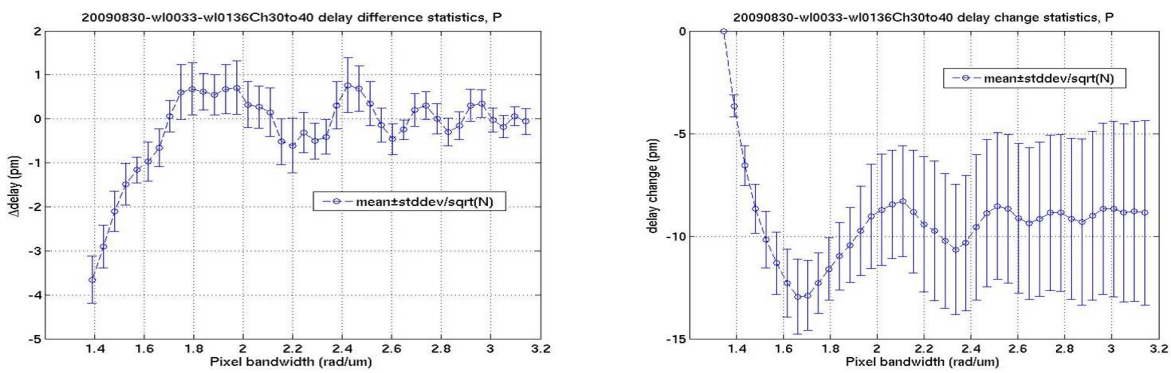

Figure 10. Contributions to fringe phase delay from individual quanta of the discretized wave numbers. (left) Cumulative contributions as increasing the bandwidth to include more quanta.

and narrow angle observations is different. Using model to estimate these error is currently an on-going activity. In the future, we expect to make use this estimations to correct errors due to pointing errors or mitigate their impact in data processing.

3.2 Sensitivity to bandwidth used in the fringe model

The core of the spectral calibration is to use fringe model to synthesize fringes for different spectra to compensate the effect due to spectral difference in the observed fringes. The fringe model contains an integration over wave number for synthesizing fringes. An important parameter affecting the fringe model usage is the bandwidth over which the integration is done. In absence of errors, we would like to include as much as bandwidth in the model as possible to avoid truncation error. However, as we increase the band to include more signal, we also pick up more noise. Therefore, we need to balance the systematic and random error to choose an optimal bandwidth for the model. In view of Eq. (7), the integration is done as a sum over discrete frequency components. Left plot in Fig. 10 shows the contributions from consecutive discrete frequency components to the calibration errors. The random errors are estimated using the variations between different long stroke measurements. The cumulative contributions, as we expand the band for model fringe computation by including more frequency components, are displayed in the right plot in Fig. 10.

We now show how we choose the bandwidth to be 2.8 rad/um. Let the contribution from the n-th quanta is expressed as

$$\Delta d_n = b_n + \epsilon_n \tag{11}$$

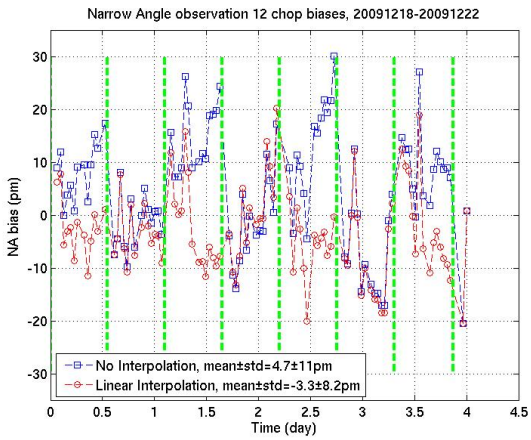

Figure 11. Calibration errors with and without instrument calibration interpolation

where b_n is the systematic bias and ϵ_n represents random error with zero mean and standard deviation σ_n. We assume $b_n \to 0$ as $n \to \infty$. It is convenient to define the bias up to including n-th quanta

$$B_n \equiv \sum_{m=n+1}^{\infty} b_n \,, \tag{12}$$

to have $B_n \to 0$ as $n \to \infty$. The RMS of the error for including up to n-th term is

$$\mathrm{RMS}_n = B_n^2 + \sum_{m=1}^{n} \sigma_n^2 \,. \tag{13}$$

If $B_{n+1}^2 - B_n^2 < \sigma_{n+1}^2$, we have $\mathrm{RMS}_{n+1} > \mathrm{RMS}_n$. Now suppose for certain M, $B_{n+1}^2 - B_n^2 < \sigma_{n+1}^2$ holds for $n > M$, we shall choose M to be the cutoff of the bandwidth. Using this as a guideline, according to Fig. 10, we simply picked up 2.8 rad/um as our bandwidth because as the bandwidth goes beyond 2.8 rad/um, the improvement on biases as shown in the cumulative curve at right curve is no more than the uncertainty of each quanta as shown by the error bar in the left plot in Fig. 10.

3.3 Interpolation of instrument calibration to remove drift error

The system instability leads to calibration errors from the change of instrument property between the instrument calibration and the narrow angle observation. On SCDU, we found that most of the system variations are caused by thermal environmental changes, typically happening at time scale of a day. The nominal SIM observation plan has daily instrument calibration. Because the thermal driven system changes are mostly low frequency variations over time, we use a linear interpolation of the instrument calibrations to remove the error due to any linear drift between the instrument calibrations. It is possible to use a higher order polynomials to remove higher order drifts.This however also introduce more uncertainties into the interpolation. So far, we have not done much research along this thread. The instrument calibration may be described as

$$\mathrm{instrument}(t_{\mathrm{NA}}) = \mathrm{instrument}(t_1)\frac{t_2 - t_{\mathrm{NA}}}{t_2 - t_1} + \mathrm{instrument}(t_2)\frac{t_{\mathrm{NA}} - t_1}{t_2 - t_1} \tag{14}$$

where "instrument" refers to instrument properties relevant to spectral calibration, i.e the complex instrument responses as estimated by the Discrete Fourier Transform of the long stroke fringes. Using this interpolation, we can remove some errors due to system drifts for spectral calibration. Fig. 11 shows the results before and after the interpolation and the RMS of errors is reduced from 11pm to 8.2pm. This shows roughly 7pm drift has been removed from the RMS.

4. SUMMARY AND FUTURE WORK

We have conducted sensitivity studies regarding errors in applying the spectral calibration and estimation scheme and made improvements to achieve better performance. The pointing sensitivity studies enable us to explain the observed bias shifts in 2007 as well as the large channel OPD bias variation across the spectral channels. Correcting systematic pointing errors and improving pointing sensitivities reduces the systematic error to less than 3pm. Improving pointing sensitivities helps also reducing systematic errors due to system instability. It is possible to use long stroke fringe measurements and fringe model to estimate pointing sensitivities and channel OPD errors due to the pointing errors.

We also did a trade study between systematic error and random error is presented for determining the bandwidth used in the fringe model for spectral calibration. We also demonstrated the efficacy of using an interpolation of instrument calibration to remove calibration errors due to system drift.

With all these improvements, the SCDU test bed has successfully demonstrated that SIM-Lite missions can met the 1pm noise floor requirement for detecting earth-like exoplanets.

Future work would be further improve the estimation of the pointing sensitivities using long stroke fringe measurements and mitigate impact of pointing errors in data processing.

Acknowledgments

This work was prepared at the Jet Propulsion Laboratory, California Institute of Technology, under a contract with the National Aeronautics and Space Administration.

REFERENCES

[1] R. Demers, X. An, A. Azizi, G. Brack, O. Lay, D. Ryan, T. Shen, G. Sun, H. Tang, C. Zhai, "Spectral calibration at the picometer level on SCDU(Spectral calibration development unit)," SPIE 2008 Astronomical Telescopes and Instrumentation, Marseille, France, (2008).

[2] C. Zhai, J. Yu, M. Shao, R. Goullioud, M. Milman, and T. Shen, SIM PlanetQuest white-light fringe modeling: picometer accuracy calibration and estimation algorithms, Applied Optics, 48, 847 (2009).

[3] B. Nemati, T.P. Shen, X. An, R. Goullioud, M. Shao, U.J. Wehmeier, M.A. Weilert, T.A. Werne, J. P. Wu, *Mitigation of Angle Tracking Errors due to Color Dependent Centroid Shifts in SIM-Lite*, SPIE 2010 Astronomical Telescopes and Instrumentation, San Deigo, CA, (2010).

[4] B. Nemati, X. An, R. Goullioud, M. Shao, T.J. Shen, U.J. Wehmeier, X. Wang, M.A. Weilert, T.A. Werne, J.P. Wu, C. Zhai, *SIM interferometer testbed (SCDU) status and recent results* SPIE 2010 Astronomical Telescopes and Instrumentation, San Deigo, CA, (2010).

[5] X. Wang, X. An, R. Goullioud, B. Nemati, M. Shao, T.J. Shen, U.J. Wehmeier, M.A. Weilert, T.A. Werne, J.P. Wu, C. Zhai, *SCDU testbed narrow angle astrometric performance*, SPIE 2010 Astronomical Telescopes and Instrumentation, San Deigo, CA, (2010).